

NullSpaceNet: Nullspace Convolutional Neural Network with Differentiable Loss Function

Mohamed H. Abdelpakey^{1,2} and Mohamed S. Shehata^{1,2}

¹ University of British Columbia,

Department of Computer Science, Math, Physics, and Statistics.

Kelowna, BC, Canada

² Memorial University of Newfoundland,

Computer Engineering and Applied Science, St. John's, NL, Canada

{mohamed.abdelpakey,mohamed.sami.shehata}@ubc.ca

Paper ID

Abstract. We propose NullSpaceNet, a novel network that maps from the pixel level input to a joint-nullspace (as opposed to the traditional feature space), where the newly learned joint-nullspace features have clearer interpretation and are more separable. NullSpaceNet ensures that all inputs from the same class are collapsed into one point in this new joint-nullspace, and the different classes are collapsed into different points with high separation margins. Moreover, a novel differentiable loss function is proposed that has a closed-form solution with no free-parameters. NullSpaceNet exhibits superior performance when tested against VGG16 with fully-connected layer over 4 different datasets, with accuracy gain of up to 4.55%, a reduction in learnable parameters from $\sim 135M$ to $\sim 19M$, and reduction in inference time of $\sim 99\%$ in favor of NullSpaceNet. This means that NullSpaceNet needs less than 1% of the time it takes a traditional CNN to classify a batch of images with better accuracy.

Keywords: Feature Learning, Convolutional Neural Network, Joint-Nullspace.

1 Introduction

In recent years, Convolutional Neural Networks (CNNs) have revolutionized computer vision tasks such as object tracking [1,2,29,3], surveillance systems [19], image understanding [25], computer interactions [30] and generative models [17]. Image classification is one of the core tasks in computer vision, especially in Large Scale Visual Recognition Challenges (e.g., ILSVRC15) [35]. Most classification networks consist of two parts: 1) the feature extractor and 2) the classifier. The feature extractor uses a stack of convolutional layers to extract the deep features from the input images through consecutive convolutional operations. The classifier uses fully-connected layers with a softmax layer. It has been proven that most of the network's learnable parameters are located in the fully

connected layers [23]. For example, the classifier in VGG16 has 102.76 million parameters, while the feature extractor has only 32 million parameters. Consequently, this huge amount of learnable parameters causes a heavy load in the training phase.

In this paper, we propose NullSpaceNet, a novel network that maps from the input pixel level to a joint-nullspace, as opposed to a traditional CNN that maps the input pixel level to a feature space. The newly learned nullspace features have a clear interpretation and are more separable. In particular, instead of using the fully connected layers with the categorical cross-entropy to maximize the likelihood between the estimated class probabilities and the true probability of the correct class, NullSpaceNet projects the pixel level inputs onto a joint-nullspace. All inputs from the same class are collapsed into one point in this new joint-nullspace and the different classes are collapsed into different points with high separation margins. Moreover, the hyperplane that has the orthonormal vectors of the projected nullspace features is well-defined and can be described as shown in Eq. 22 and Fig. 2. In contrast to a traditional CNN used in a classification task, which optimizes its weights by maximizing the likelihood between the estimated class probability of the network’s output and the true probability, NullSpaceNet minimizes the within-class scatter matrix (to be zero or very close to zero), while maintaining the between-class scatter matrix to be always positive. This makes the classification task more robust as shown in Fig. 3 (a) and Fig. 3 (b). The results are available online ¹

To summarize, the main contributions of this paper are three-fold:

1. A novel Network (NullSpaceNet) that learns to map from the input pixel level to a joint-nullspace. The formulation of NullSpaceNet ensures that the nullspace features from the same class are collapsed into a single point while the ones from different classes are collapsed into different points.
2. A differentiable loss function is developed to train NullSpaceNet. The proposed loss function is different from the standard categorical cross-entropy. The proposed loss function ensures that the within-class scatter matrix vanishes while maintaining a positive between-class scatter matrix.
3. The proposed NullSpaceNet has a clear interpretation, both mathematically and geometrically.

The effect of these three contributions result in accuracy gain of up to 4.55%, a reduction in learnable parameters from $\sim 135M$ to $\sim 19M$, and reduction in inference time of $\sim 99\%$ in favor of NullSpaceNet. This means that NullSpaceNet needs less than 1% of the time it takes a traditional CNN to classify a batch of images with better accuracy over all 4 datasets we used in testing.

The rest of the paper is organized as follows: Related work is presented in section 2, then section 3 details the proposed NullSpaceNet. The training and inference phases are presented in section 4. The experimental results are presented in section 5. Finally, section 6 concludes the paper.

¹ <https://github.com/NullSpaceNet>

2 Related Work

Linear Discriminant Analysis (LDA) and nullspace have existed as analytical methods for a significant period of time [40,12,34,24,9,7]. LDA has been frequently been employed as a dimensionality reduction tool or feature extractor within the field of classification [14,38,16,15,15,10,37,21,28,26]. Nullspace can be derived from the Fisher-criterion objective function in an analytical way. This work [8] used multiple local nullspaces to detect the small moving objects in aerial videos. Using the nullspace allows the detector to nullify the background while maintaining the moving objects.

Nullspace has been used in [27] to specify whether the incoming data belongs to the existing class or not. In particular, they used Incremental Kernel Nullspace Discriminative (IKNDA). To speedup their method, an intelligent update scheme is used to extract information from newly added samples. The work in [32] proposed Max-Mahalanobis distribution (MMD) using LDA to improve the robustness of the adversarial attack. [39] proposed to learn a capsule subspace using orthogonal projection. The length of the resultant capsules is utilized to score the probability of belonging to different categories. The authors in [31] proposed to apply the Hybrid Orthogonal Projection Estimation (HOPE) to CNN for image classification. HOPE is a hybrid model that combines orthogonal linear projection, for feature extraction, with mixture models. The idea in HOPE to allow for extraction of useful information from high-dimension feature vectors while filtering out irrelevant noise. [36] used LDA with the Fisher-criterion on VGG16 to classify facial gender. LDA was applied on the output of the last layer to derive a light weight version of VGG16. A Bayesian classification is then used to classify the output. Notice that, this is completely different from NullSpaceNet, where we reformulate the learning process in a differentiable way to train the network to learn a joint-nullspace. DeepLDA [6] proposed to use LDA to learn to maximize eigenvalues of the Fisher-criterion. After training, DeepLDA uses the entire training set to extract the dominant basis vectors to project the new samples. In contrast to all previous methods, we use the nullspace in VGG16 in a learnable way with a differentiable loss function to project the pixel level input to a joint-nullspace.

The only work we found that included using LDA in a deep learning framework was presented in [6], where the authors solved the LDA and integrated it in a deep CNN. It is worth mentioning that the work in [6] did not include any reference to any usage of nullspace. In our work, we do not solve for the LDA, instead we reformulate the problem within the nullspace to train the network to project from the pixel level onto the joint-nullspace.

3 Proposed Method: NullSpaceNet

3.1 Problem Definition

Given a dataset of training images $X = \{x_1, x_2, \dots, x_N\} \in \mathbb{R}^{w \times h \times d}$, where w, h and d are the width, height, and depth of each image, respectively and N is

the number of images in the training dataset. Each image is associated with a respective class C , where $C = \{c_1, c_2, \dots, c_n\} \in \mathbb{R}$, n is the number of classes in the training dataset. In this paper, we use the VGG16 as the backbone network, hence, the training images will be fed into the feature extractor part $\phi(x; \theta)$. The objective is to force the network to learn a joint-nullspace that maps from the pixel level to a strong discriminative nullspace. The learned nullspace will replace the classifier part, which has the most network’s learnable parameters.

3.2 Proposed Architecture

NullSpaceNet inherits its architecture from VGG16 . Our contribution is the addition of the nullspace layer as shown in Fig. 1 . Also, we added a (Conv-BatchNormalization-ReLU) layer with kernel size=3 to produce a 2D tensor of shape 1×800 before the nullspace layer, in the case of STL10 dataset. In the case of CIFAR10 and CIFAR100, we change the kernel size=1 of the last layer. NullSpaceNet has 19 layers, each layer consists of (Conv-BatchNormalization-ReLU), we consider the pooling as a stand-alone layer.

The novelty of NullSpaceNet lies in the nullspace layer and the differentiable loss function we propose in section 3.3. The nullspace layer forces the network, through the backpropagation, to learn the projection from the input pixel level onto a joint-nullspace, where the joint-nullspace features have optimal separation margins. The Nullspace layer achieves this through spanning vectors of the optimal within-class scatter matrix as it will be discussed in more details in section 3.3. Formulating the nullspace layer in this way prevents the network from the Small Sample Size (SSS) problem (i.e., the model has a high dimensional output features while training on small batches of images).

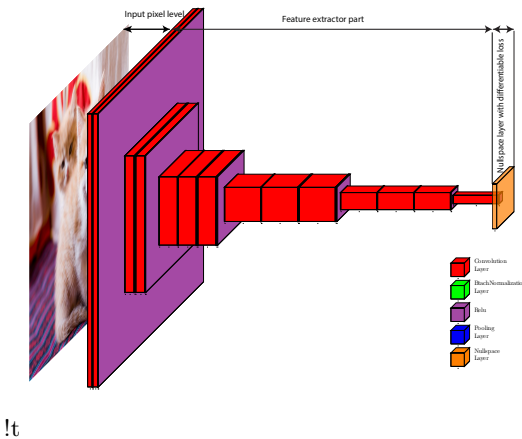


Fig. 1: NullSpaceNet architecture, the feature extractor part is inherited from VGG16. The NullSpace layer is at the end of the architecture. Note that the nullspace layer has been magnified for the sake of visualization.

3.3 Mathematical Formulation of The Loss Function

Background: To derive a differentiable loss function to train the joint-nullspace, we start from the linear discriminant analysis (LDA) [11]. In this paper, we assume that the output of the feature extractor part in the network for each image is $F \in \mathbb{R}^{D \times 1}$, where D is the depth of the output. The objective of the LDA is to find a projection matrix $P \in \mathbb{R}^{D \times M}$ that minimizes the within-class scatter matrix and maximizes the between-class scatter matrix simultaneously. This can be achieved by maximizing the Fisher-discriminant criterion $\mathcal{J}(P)$ as follows:

$$\mathcal{J}(P) = \frac{P^\top S_b P}{P^\top S_w P} \quad (1)$$

Where P is the projection matrix, S_b and S_w are the between-class and within-class scatter matrices, respectively. The optimization of Eq. 1 can be solved for the generalized eigenvalue problem as follows:

$$S_b P = \lambda S_w P \quad (2)$$

where λ is the eigenvalue of the eigenvector $S_w^{-1} S_b$.

Derivation of the proposed novel loss function:

Lemma 1: By investigating the output of the network’s feature extractor, it turns out that the network has a tendency to minimize the within-class scatter matrix, which is the constraint in the denominator of Eq. 1. However, it does not put constraints on the between-class scatter matrix as shown in Fig. 3(b).

Proof: The visualization in Fig. 3 (b). The learned features of VGG16 with FC layer are scattered with no constraints on the between-class scattered matrix where some classes (e.g., class #4, #5 and class #2 and #8) are overlapped. Based on Lemma 1, we force two constraints on the learning process. In particular, we force the between-class scatter matrix to always be positive while minimizing the within-class scatter matrix to be zero as follows:

$$P^\top S_b P > 0 \quad (3)$$

$$P^\top S_w P = 0 \quad (4)$$

Lemma 2: When the network satisfies the two constraints in Lemma 1, the distribution of the same class features in the new joint-nullspace approaches the Dirac Delta function.

Proof: Assuming the features are represented by the normal distribution, for simplicity, we will use a 1-D dimensional normal distribution.

$$\int g(\bar{x}) f(\bar{x} | \bar{\mu}, \bar{\sigma}^2) d\bar{x} \quad (5)$$

where $g(\bar{x})$ is the mean value function of the projected features by the network onto the joint-nullspace and $\bar{\sigma}$ is the standard deviation of the distribution. We

take the limit of Eq. 5 as $\bar{\sigma}^2$ approaches 0.

$$\lim_{\bar{\sigma}^2 \rightarrow 0} \left(\int g(\bar{x}) f(\bar{x} | \bar{\mu}, 0) d\bar{x} \right) = \int g(\bar{x}) \delta(\bar{x} - \bar{\mu}) d\bar{x} = g(\bar{\mu}) \quad (6)$$

Using Lemma 1 and Lemma 2 to find the limit of Eq. 1 (which guarantee the best separability as explained above), we get:

$$\lim_{(P^T S_w P) \rightarrow 0} \mathcal{J}(P) = \infty \quad (7)$$

Since the between-class scatter matrix S_b in Eq. 3 is hard to calculate, especially in the case of high dimensional features, we calculate S_b using the total-class scatter matrix S_t and the within-class scatter matrix S_w (see Eq. 10 for mathematical definition of them) as follows:

$$S_b = S_t - S_w \quad (8)$$

By substituting Eq.8 in Eq. 4 we get (since the derivation is long we will provide the details in the supplementary material):

$$P^T S_t P > 0 \quad (9)$$

Since the output of the NullSpaceNet is $f \in \mathbb{R}^{D \times N}$ when the input batch images $X \in \mathbb{R}^{w \times h \times d \times N}$, where N is the number of images. We define the within-class scatter matrix S_w and the total-class scatter matrix S_t from the output of NullSpaceNet as follows:

$$S_w = \frac{1}{N} F_w^T F_w, \quad S_t = \frac{1}{N} F_t^T F_t \quad (10)$$

where F_w is the centered class mean output features (i.e, subtracting the class mean from each feature output belonging to this class), and F_t is the centered global mean output features as shown in Eq. 11.

$$F_w = \frac{1}{N} (X - \mu_c)^T, \quad F_t = \frac{1}{N} (X - \mu_g)^T \quad (11)$$

Where μ_c is the class mean and μ_g is the global mean of the dataset.

Now, we want to integrate the scatter matrices we derived in Eq. 10 in the joint-nullspace formulation. Let U_t denote the nullspace of the total-class scatter matrix and U_w denote the nullspace of within-class matrix. From the definition of the nullspace and using the fact that S_t is non-negative definite, we get:

$$\begin{aligned} U_t &= \{u \in \mathbb{R}^D \mid S_t u = 0\} = \{u \in \mathbb{R}^D \mid u^T S_t u = 0\} \\ &= \{u \in \mathbb{R}^D \mid (F_t u)^T F_t u = 0\} \\ &= \{u \in \mathbb{R}^D \mid F_t u = 0\}. \end{aligned} \quad (12)$$

similarly, we get U_w (details are provided in the supplementary material).

Lemma 3: The projection matrix P that satisfies the constraints in Eq. 3 and Eq. 4 can be achieved, if and only if, P lies in the shared space between U_t^\perp and U_w as shown in Eq. 13.

$$P \in (U_t^\perp \cap U_w). \quad (13)$$

where U_t^\perp is the orthogonal complement subspace of U_t spanned by the centered global mean output features, it can be obtained using the Gram-Schmidt process [18].

Proof: Geometrically by looking at Eq. 12 and U_w , the only space that satisfies $S_t u = 0$ and $S_w u = 0$ is the joint-space where U_t^\perp and U_w are overlapped [14]. Now we have the nullspace of S_w which is U_w and the nullspace of S_t which is U_t . One problem with the calculation the nullspace of S_w is that the dimensionality of nullspace is at least $(D + C - n)$, where D is data dimensionality (which is high when we use the output of NullSpaceNet, e.g., 2048), C is the number of classes, and n is the sample sizes as it has been proved in [4]. To address this problem, we revert to Eq. 8 where it can be seen that S_t is the intersection of the nullspace of S_b and the nullspace of S_w . Hence, the nullspace of S_t can be removed based on this observation. We proceed with the solution using the Singular Value Decomposition (SVD) theory to decompose F_t (which was introduced in Eq. 11) as follows:

$$F_t = U \Sigma V^T \quad (14)$$

Where U and V are orthogonal.

$$\Sigma = \begin{pmatrix} \Sigma_t & 0 \\ 0 & 0 \end{pmatrix} \quad (15)$$

Σ_t is the diagonal matrix $\Sigma_t \in \mathbb{R}^{t \times t}$ with the eigenvalues. Now we can represent S_t as follows:

$$\begin{aligned} S_t &= F_t F_t^T \\ &= V \Sigma^T U^T U \Sigma V^T \\ &= U \Sigma \Sigma^T U^T \\ &= U \begin{pmatrix} \Sigma_t^2 & 0 \\ 0 & 0 \end{pmatrix} U^T \end{aligned} \quad (16)$$

We select a part of orthogonal basis of U with dimension $U_1 \in \mathbb{R}^{m \times t}$ where $t = \text{RANK}(S_t)$, using the new subspace U_1 spanned by the new set of the orthogonal basis we project the scatter matrices as follows:

$$\tilde{S}_b = U_1 S_b U_1^T, \tilde{S}_w = U_1 S_w U_1^T, \text{ and } \tilde{S}_t = U_1 S_t U_1^T \quad (17)$$

Where $\tilde{(\cdot)}$ represents the reduced version of the decomposed $S_b, S_w, \text{ and } S_t$.

From Eq. 14 and Eq. 17 we can apply the SVD again on F_t with complexity

of $O(Dn^2)$ instead of $O(D^2n)$. Now instead of calculating the nullspace of S_w , we can calculate the nullspace of \tilde{S}_w as shown in Eq. 18. This gives the network two advantages: 1) the model does not suffer from the small sample size (SSS) problem, e.g., the model has a high dimensional output features while training on small batches of images, as in [6], and 2) it is faster than solving the generalized eigenvalue problem.

$$W = \text{Span}(\tilde{S}_w) \quad (18)$$

Where W is the nullspace of \tilde{S}_w . Finally, the projection matrix that satisfies Eq. 3 and Eq. 4 can be calculated by:

$$P = W \times M \quad (19)$$

Where M is the eigenvectors of $W^T \tilde{S}_b W$ corresponding to the non-zero eigenvalues.

Algorithm 1 Steps to Calculate the Proposed Loss Function

input : The output of the last layer of VGG16 $F \in \mathbb{R}^{D \times N}$

output: Optimize the weights of the NullSpaceNet using the proposed differentiable loss function \mathcal{L} based on the nullspace formulation

- 1: Calculate matrix F_t ;
 - 2: Calculate $SVD(F_t^T)$;
 - 3: Calculate the scatter matrices S_w, S_b, S_t ;
 - 4: Calculate matrices $\tilde{S}_t, \tilde{S}_b, \tilde{S}_w$ from Eq. 17;
 - 5: Calculate the nullspace W of \tilde{S}_w using Eq. 18;
 - 6: Solve for the eigenvalues of $W^T \tilde{S}_b W$;
 - 7: Formulate the loss function over the average of the non-zero eigenvalues from the last step using Eq. 20;
 - 8: Use the proposed differentiable loss function in Eqs. 20 and 21 to train the network
-

3.4 Gradient of the Loss Function

Training the NullSpaceNet requires the loss function to be differentiable everywhere. Hence, we propose a novel differentiable loss function that maximizes the positive (or minimizes the negative) of the average non-zero eigenvalues of the decomposed $W^T \tilde{S}_b W$. We define k as the number of eigenvalues in two cases: 1) when $\{E_1, \dots, E_{c-1}\} > 0$, and 2) when $\{E_k, \dots, E_{c-1}\} < 0$. The steps to calculate the proposed differentiable loss function is shown in Alg. 1. The final equation of these steps is shown in Eq. 20.

$$\mathcal{L}(\phi(E; \theta)) = - \sum_{i=1}^k SVD_{E_i}(W^T \tilde{S}_b W) \quad (20)$$

Where $E \in \{E_1, \dots, E_k\} = \{E_j | E_j < \min\{E_1, \dots, E_{C-1}\} + \epsilon\}$.

Using the chain rule, the derivative of the loss function in Eq. 20 w.r.t the last

layer H of NullSpaceNet is given by Eq. 21 (details are given in the supplementary materials).

$$\frac{\partial \mathcal{L}}{\partial H} = - \frac{\sum_{i=1}^k \frac{\partial SVD_{E_i}(W^T \tilde{S}_b W)}{\sum_{i=1}^k \psi_i^T \left(\frac{\partial \tilde{S}_b}{\partial H} - \psi_i \frac{\partial \tilde{S}_w}{\partial H} \right) \psi_i}}{\sum_{i=1}^k \psi_i^T \left(\frac{\partial \tilde{S}_b}{\partial H} - E_i \frac{\partial \tilde{S}_w}{\partial H} \right) \psi_i} \times \frac{\partial H}{\partial H} \quad (21)$$

Where ψ_i are the Eigenvectors associated with the Eigenvalues E_i

3.5 Insights into NullSpaceNet

In this section, we provide a deeper look, both mathematically and geometrically, into the proposed NullSpaceNet.

Mathematical Insights: The main idea of NullSpaceNet is to learn to project the input data onto another subspace (different from the traditional feature space) that satisfies the two constraints in Eq. 3 and Eq. 4. The new proposed subspace (i.e., joint-nullspace) mathematically forces the within-class scatter matrix to vanish through the optimization of the proposed loss function in Eqs. 20 and 21. Meanwhile the new joint-nullspace mathematically forces the between-class scatter matrix to always be positive through the optimization of the loss function in Eq. 20.

Geometric Insights: The features that are produced by NullSpaceNet are living in the hyperplane represented by $U_t^\perp \cap U_w$, and all inputs from the same class are collapsed into one point, while the inputs from different classes are collapsed into different points as shown in Fig. 2. The hyperplane now is well-defined and all the features are located in a confined space that can be precisely described both mathematically and geometrically.

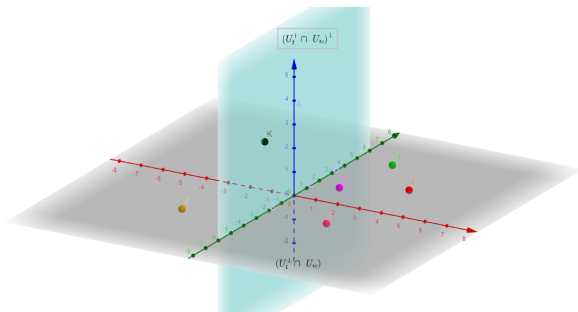


Fig. 2: Geometric illustration of the learned feature projected by the network in the joint-nullspace. Each color associated with a letter encodes a class, note that all inputs from the same class are collapsed into a single point. Notice that all classes exist on the Grey-colored hyperplane ($U_t^\perp \cap U_w$) including point k .

4 Training and Inference of NullSpaceNet

4.1 NullSpaceNet Training Phase

Firstly, the input batch of images is fed into the input layer as shown in Fig. . 1. The batch undergoes the operation of the layers such as convolution, normalization, and pooling, then to the nullspace layer, where all calculations and the loss function are performed as shown in Alg. 1.

4.2 NullSpaceNet Inference Phase

Even though the training phase does not require a special setup, the inference phase in the NullSpaceNet is different. After the network is trained using the proposed differentiable loss function in Eq. 20, we feed the entire training set into NullSpaceNet, then extract the output mean of each class from the last layer $\mu_k = (\mu_1, \dots, \mu_C)$ that has the dimension $\mathcal{R}^{D \times N}$, where N is the number of images. The eigenvectors of the decomposed $W^T \tilde{S}_b W$ will be calculated, the number of the basis vectors are $C - 1$, where C is the number of training classes. From Eq. 19, the projection matrix P is calculated. Using the hyperplane equation, any output of the testing dataset t^T can be classified using the hyperplane equation [13] (Eq. 22) below:

$$\operatorname{argmax}_k \beta_k(t) = t^T \Sigma^{-1} \mu_k - \frac{1}{2} \mu_k^T \Sigma^{-1} \mu_k \quad (22)$$

Where $\Sigma = P \times P^T$ and β is the hyperplane.

5 Experimental Results

Implementation Details

NullSpaceNet has been implemented in Python using PyTorch framework [33]. All experiments have been performed on Linux with Xeon E5 @2.20 GHz CPU and NVIDIA Titan XP GPU. All experiments are performed on networks trained from scratch. We set ϵ to 1 and the number of epochs for the training to 200. We used Adam optimizer [20] with learning rate of 0.0001, a momentum of 0.9, and a batch size of 400 images.

Datasets

The datasets CIFAR10 and CIFAR100 [22] have resolution of 32×32 . CIFAR10 has 10 classes collected from natural images, while CIFAR100 has 100 classes. Each dataset has 50,000 images for training and 10,000 images for testing. We used 49,000 for training, 1,000 for validation and 10,000 for testing for both datasets. STL10 dataset [5] has 10 classes with higher image resolutions, in contrast to CIFAR datasets, to show the effect of higher image resolution on the performance. STL10 has 5,000 images for training, while the testing set has 8,000 images. We used 5,000 for training set, 1,000 for validation set from the testing set and the remaining 7,000 for testing.

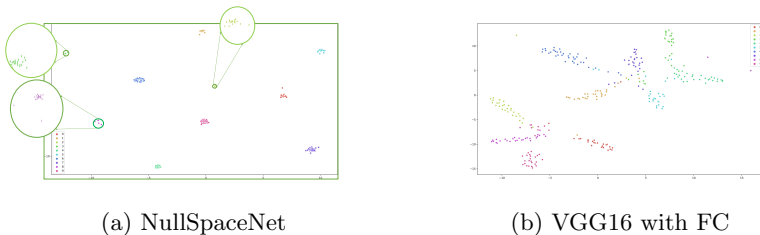


Fig. 3: t-SNE visualization of the learned features on STL10 dataset using (a) NullSpaceNet, (b) VGG16 with FC layer.

Results on CIFAR10 Dataset

The results on CIFAR10 dataset are shown in Table 1. VGG16 with fully-connected (FC) layer and categorical-cross entropy achieves a test accuracy of 93.51%, while the proposed NullSpaceNet achieves 94.01%.

The accuracy difference between the proposed NullSpaceNet and the VGG16 with FC layer is $\sim 0.5\%$, in favor of NullSpaceNet. More importantly, there is a significant reduction in the network parameters of NullSpaceNet compared to VGG16 with FC layer. The parameters went down from ~ 134 million in VGG16 with FC layer to ~ 18 million in NullSpaceNet, which is a reduction of 92.99%. Table 3 shows the inference time required per batch (2000 images), the time required by VGG16 with FC is 0.6841 seconds while NullSpaceNet required only 0.0051 seconds, which is a reduction of 99.25% in favor of NullSpaceNet.

Results on CIFAR100 Dataset

The results on CIFAR100 dataset are shown in Table 2. NullSpaceNet outperforms VGG16 with FC layer by 0.07%; still the gain is not significant similar to the CIFAR10 dataset. But, the number of parameters in NullSpaceNet has been reduced from ~ 134 millions to ~ 18 million parameters. Table 3 shows the inference time required per batch (2000 images), the time required by VGG16 with FC is 0.6841 seconds while NullSpaceNet required only 0.0051 seconds, which is a reduction of 99.25% in favor of NullSpaceNet.

The importance of conducting this experiment on CIFAR100 dataset is to prove that NullSpaceNet performance is not affected by the increase in the number of classes in the classification task.

Results on STL10 Dataset

The results on STL10 dataset are shown in Tables 4 and 5. NullSpaceNet outperforms VGG16 with FC layer in terms of accuracy with gain of 2.57%, parameters reduction of 92.99%, and inference time reduction of 99.22%. It is worth noting that NullSpaceNet significantly benefits from the higher image resolution, STL10 has images resolution of 64×64 .

To visualize the learned features by NullSpaceNet and VGG16 with FC layer on STL10 dataset, t-SNE is used to provide Fig. 3. Each color is associated with a number that represents a class in the STL10 dataset. It can be seen from Fig. 3(a) that the within-class scatter matrix for all classes has been reduced to minimum and the between-class scatter maximized the margin separation between class.

By examining Fig. 3(b), the classes are overlapping and the separation margin is not optimal. Fig. 3 visualizes the power of the new proposed NullSpaceNet.

Results on ImageNet

Results on ImageNet are shown in Table 7. Note that we used only 50,000 images from ImageNet. ImageNet has a higher resolution compared to CIFAR datasets and STL10, we have downscaled all images to be 128×128 . The number of parameters have increased from ~ 134 to ~ 135 in VGG16+FC, while it went up from ~ 18 to ~ 19 in the case of NullSpaceNet. AS it can be seen from Table 7, the accuracy gain is more evident in favor of NullSpaceNet, as the resolution increases. NullSpaceNet has an accuracy of 98.87% compared to 94.32% in VGG16+FC, which is a gain of +4.55%. The inference time for VGG16+FC is 1.5653 seconds per batch, while NullSpaceNet needed only 0.0168 seconds, which is a reduction of 98.92%.

Effect of Image Resolution

The accuracy gain between the proposed NullSpaceNet and the VGG16 with FC layer when tested on CIFAR10 and CIFAR100 is 0.5% and 0.07%, respectively, in favor of NullSpaceNet. The gain suggests that the accuracy does not significantly benefit from the projection onto the proposed joint-nullspace in this case. This can be justified based on the fact that the images resolution in CIFAR10 and CIFAR100 is 32×32 . This means that the number of pixel level features to be mapped in either the feature space or the joint-null space is small, and hence explains the small accuracy gain.

This justification is further supported in lights of the results on the STL10 dataset (which has higher images resolution 64×64), and consequently better accuracy in favor of NullSpaceNet. Furthermore, another experiment has been performed on a reduced resolution version of STL10 dataset. All training images have been reduced to 32×32 resolution, similar to CIFAR10 and CIFAR100 dataset. NullSpaceNet has been trained on the modified version STL10, and the results are shown in Table 6. It is seen that the accuracy gain is similar to the ones in CIFAR10 and CIFAR100. Another experiment has been conducted on ImageNet, the results are shown in table 7 and it shows a ccuracy difference of 4.55%. This confirms our justification that NullSpaceNet power becomes more clear in cases of images with higher resolution. In general, NullSpaceNet will outperform VGG16 with FC layer in all cases. All results are summarized in table 8

Top-k Error Rate on STL10

Top-k error rate is the fraction of the testing set for which the true label is not among the five labels that are most likely by the model prediction [23]. The top row shows the training and testing loss. In the bottom row, we report the top-1 and top-5 accuracy on the STL10 dataset.

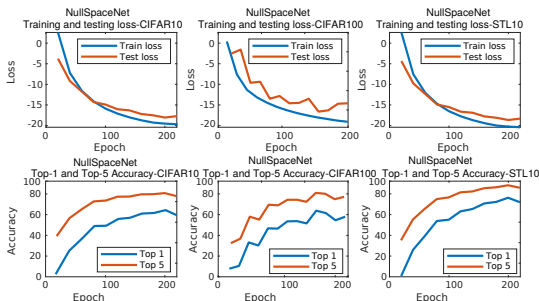


Fig. 4: Accuracies and Losses on CIFAR10, CIFAR100, and STL10 - Top row: Training and testing losses, Bottom row: the top-1 and top-5 accuracy.

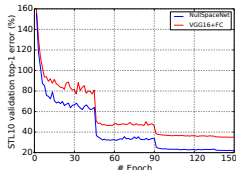


Fig. 5: Top-1 error on the validation set of STL10. At the beginning, NullSpaceNet and VGG16+FC have almost the same error rate, then NullSpaceNet has lower error rate as the number of epochs increase.

Table 1: Test Accuracy on CIFAR10.

Architecture	Accuracy	# Parameters
VGG16 + FC (cross-entropy loss)	93.51%	134,309,962
NullSpaceNet (Proposed)	94.01%	18,411,936

6 Conclusions and Future Work

A typical CNN optimizes the weights of the network by maximizing the likelihood between the estimated probability of the predicted class and the true probability of the correct class. In contrast, NullSpaceNet learns to project the features from the pixel level (i.e, input image) onto a joint-nullspace. All features from the same class are collapsed into a single point in the learned joint-nullspace, whereas all features from different classes are collapsed into different points with high separation margins. Also, a novel differentiable loss function is developed to train NullSpaceNet to learn to project the features onto the joint-nullspace. NullSpaceNet with the proposed differentiable loss function exhibits a superior performance, with accuracy gain of 0.07 – 2.57%, and reduction in inference time of 99.22 – 99.25% in favor of NullSpaceNet. This means that NullSpaceNet needs less than 1% of the time it takes a traditional CNN to classify a batch of images with slightly better accuracy, Future work include extending this work to other fields such as object tracking.

Table 2: Test Accuracy on CIFAR100.

Architecture	Accuracy	# Parameters
VGG16 + FC (cross-entropy loss)	92.26%	134,309,962
NullSpaceNet(proposed)	92.33%	18,411,936

Table 3: Inference time and number of parameters on CIFAR10/CIFAR100

Architecture	# Parameters	Average inference time/batch
VGG16 + FC (cross-entropy loss)	134,309,962	0.6841 Seconds
NullSpaceNet(Proposed)	18,411,936	0.0051 Seconds

Table 4: Test Accuracy STL10 dataset.

Architecture	Accuracy	# Parameters
VGG16 + FC (cross-entropy loss)	93.74%	134,309,962
NullSpaceNet (proposed)	96.31%	18,411,936

Table 5: Inference time and number of parameters on STL10.

Architecture	# Parameters	Average inference time/batch
VGG16 + FC (cross-entropy loss)	134,309,962	1.3487 Seconds
NullSpaceNet(Proposed)	18,411,936	0.0105 Seconds

Table 6: Test Accuracy on modified version of STL10 (32×32).

Architecture	Accuracy	# Parameters
VGG16 + FC (cross-entropy loss)	93.89%	134,309,962
NullSpaceNet (Proposed)	93.91%	18,411,936

Table 7: Test Accuracy on ImageNet dataset with image resolution 128×128 . Only 50,000 images were used.

Architecture	Accuracy	# Parameters	Average Inference time/batch
VGG16 + FC (cross-entropy loss)	94.32%	135,310,123	1.5653
NullSpaceNet (Proposed)	98.87%	19,415,654	0.0168

Table 8: A summerization of the results on 4 datasets, CIFAR10, CIFAR100, STL10, and ImageNet. All results are in favor of NullSpaceNet

Dataset	Accuracy Difference	Image Size	Parameters Reduction	Time Reduction
CIFAR10	+0.5%	32×32	+86.29%	+99.25%
CIFAR100	+0.07%	32×32	+86.29%	+99.25%
STL10	+2.57%	64×64	+86.29%	+99.22%
STL10 (modified)	+0.02%	32×32	+86.29%	+99.22%
ImageNet	+4.55%	128×128	+85.65%	+98.92%

References

1. Abdelpakey, M.H., Shehata, M.S.: Domainsiam: Domain-aware siamese network for visual object tracking. In: International Symposium on Visual Computing. pp. 45–58. Springer (2019)
2. Abdelpakey, M.H., Shehata, M.S.: Dp-siam: Dynamic policy siamese network for robust object tracking. *IEEE Transactions on Image Processing* **29**, 1479–1492 (2019)
3. Bhat, G., Danelljan, M., Gool, L.V., Timofte, R.: Learning discriminative model prediction for tracking. In: Proceedings of the IEEE International Conference on Computer Vision. pp. 6182–6191 (2019)
4. Chen, L.F., Liao, H.Y.M., Ko, M.T., Lin, J.C., Yu, G.J.: A new lda-based face recognition system which can solve the small sample size problem. *Pattern recognition* **33**(10), 1713–1726 (2000)
5. Coates, A., Ng, A., Lee, H.: An analysis of single-layer networks in unsupervised feature learning. In: Proceedings of the fourteenth international conference on artificial intelligence and statistics. pp. 215–223 (2011)
6. Dorfer, M., Kelz, R., Widmer, G.: Deep linear discriminant analysis. in Proceedings of the International Conference on Learning Representations (ICML) pp. 1–13 (2016)
7. Dufrenois, F., Noyer, J.C.: A null space based one class kernel fisher discriminant. In: 2016 International Joint Conference on Neural Networks (IJCNN). pp. 3203–3210. IEEE (2016)
8. ElTantawy, A., Shehata, M.S.: Krmaro: aerial detection of small-size ground moving objects using kinematic regularization and matrix rank optimization. *IEEE Transactions on Circuits and Systems for Video Technology* **29**(6), 1672–1686 (2018)
9. ElTantawy, A., Shehata, M.S.: Local null space pursuit for real-time moving object detection in aerial surveillance. *Signal, Image and Video Processing* **14**(1), 87–95 (2020)
10. Fei, Z., Yang, E., Li, D.D.U., Butler, S., Ijomah, W., Li, X., Zhou, H.: Deep convolution network based emotion analysis towards mental health care. *Neurocomputing* (2020)
11. Foley, D.H., Sammon, J.W.: An optimal set of discriminant vectors. *IEEE Transactions on computers* **100**(3), 281–289 (1975)
12. Foster, L.V.: Rank and null space calculations using matrix decomposition without column interchanges. *Linear Algebra and its Applications* **74**, 47–71 (1986)
13. Friedman, J., Hastie, T., Tibshirani, R.: The elements of statistical learning, vol. 1. Springer series in statistics New York (2001)
14. Guo, Y.F., Wu, L., Lu, H., Feng, Z., Xue, X.: Null foley–sammon transform. *Pattern recognition* **39**(11), 2248–2251 (2006)
15. Hou, Q., Wang, Y., Jing, L., Chen, H.: Linear discriminant analysis based on kernel-based possibilistic c-means for hyperspectral images. *IEEE Geoscience and Remote Sensing Letters* **16**(8), 1259–1263 (2019)
16. Hu, P., Peng, D., Sang, Y., Xiang, Y.: Multi-view linear discriminant analysis network. *IEEE Transactions on Image Processing* **28**(11), 5352–5365 (2019)
17. Huang, H., Wang, C., Yu, P.S., Wang, C.D.: Generative dual adversarial network for generalized zero-shot learning. In: Proceedings of the IEEE conference on computer vision and pattern recognition. pp. 801–810 (2019)

18. Jensen, V.G., Jenson, H., Jeffreys, G.: *Mathematical methods in chemical engineering* (1977)
19. Kendall, A., Grimes, M., Cipolla, R.: Posenet: A convolutional network for real-time 6-dof camera relocalization. In: *Computer Vision (ICCV), 2015 IEEE International Conference on*. pp. 2938–2946. IEEE (2015)
20. Kingma, D.P., Ba, J.: Adam: A method for stochastic optimization. arXiv preprint arXiv:1412.6980 (2014)
21. Korkmaz, S.A., Bínol, H., Akçiçek, A., Korkmaz, M.F.: A expert system for stomach cancer images with artificial neural network by using hog features and linear discriminant analysis: Hog_lda_ann. In: *2017 IEEE 15th International Symposium on Intelligent Systems and Informatics (SISY)*. pp. 000327–000332. IEEE (2017)
22. Krizhevsky, A., Hinton, G., et al.: Learning multiple layers of features from tiny images (2009)
23. Krizhevsky, A., Sutskever, I., Hinton, G.E.: Imagenet classification with deep convolutional neural networks. In: *Advances in neural information processing systems*. pp. 1097–1105 (2012)
24. Kueng, R., Jung, P.: Robust nonnegative sparse recovery and the nullspace property of 0/1 measurements. *IEEE Transactions on Information Theory* **64**(2), 689–703 (2017)
25. Lenc, K., Vedaldi, A.: Understanding image representations by measuring their equivariance and equivalence. In: *Proceedings of the IEEE Conf. on Computer Vision and Pattern Recognition (CVPR)* (2015)
26. Liang, Y., Sun, L., Ser, W., Lin, F., Thng, S.T.G., Chen, Q., Lin, Z.: Classification of non-tumorous skin pigmentation disorders using voting based probabilistic linear discriminant analysis. *Computers in biology and medicine* **99**, 123–132 (2018)
27. Liu, J., Lian, Z., Wang, Y., Xiao, J.: Incremental kernel null space discriminant analysis for novelty detection. In: *Proceedings of the IEEE Conference on Computer Vision and Pattern Recognition*. pp. 792–800 (2017)
28. Mahdianpari, M., Salehi, B., Mohammadimanesh, F., Brisco, B., Mahdavi, S., Amani, M., Granger, J.E.: Fisher linear discriminant analysis of coherency matrix for wetland classification using polsar imagery. *Remote Sensing of Environment* **206**, 300–317 (2018)
29. Mohamed, M.M.: Denssiam: End-to-end densely-siamese network with self-attention model for object tracking. In: *Advances in Visual Computing: 13th International Symposium, ISVC 2018, Las Vegas, NV, USA, November 19–21, 2018, Proceedings*. vol. 11241, p. 463. Springer (2018)
30. Molchanov, P., Yang, X., Gupta, S., Kim, K., Tyree, S., Kautz, J.: Online detection and classification of dynamic hand gestures with recurrent 3d convolutional neural network. In: *Proceedings of the IEEE Conference on Computer Vision and Pattern Recognition*. pp. 4207–4215 (2016)
31. Pan, H., Jiang, H.: Learning convolutional neural networks using hybrid orthogonal projection and estimation. In: Zhang, M.L., Noh, Y.K. (eds.) *Proceedings of the Ninth Asian Conference on Machine Learning*. *Proceedings of Machine Learning Research*, vol. 77, pp. 1–16. PMLR (15–17 Nov 2017), <http://proceedings.mlr.press/v77/pan17a.html>
32. Pang, T., Du, C., Zhu, J.: Max-mahalanobis linear discriminant analysis networks. *ICML* (2018)
33. Paszke, A., Gross, S., Chintala, S., Chanan, G.: Pytorch: Tensors and dynamic neural networks in python with strong gpu acceleration. *PyTorch: Tensors and dynamic neural networks in Python with strong GPU acceleration* **6** (2017)

34. Recht, B., Xu, W., Hassibi, B.: Null space conditions and thresholds for rank minimization. *Mathematical programming* **127**(1), 175–202 (2011)
35. Russakovsky, O., Deng, J., Su, H., Krause, J., Satheesh, S., Ma, S., Huang, Z., Karpathy, A., Khosla, A., Bernstein, M., et al.: Imagenet large scale visual recognition challenge. *International Journal of Computer Vision* **115**(3), 211–252 (2015)
36. Tian, Q., Arbel, T., Clark, J.J.: Deep l₁-pruned nets for efficient facial gender classification. In: *Proceedings of the IEEE Conference on Computer Vision and Pattern Recognition Workshops*. pp. 10–19 (2017)
37. Wang, Q., Meng, Z., Li, X.: Locality adaptive discriminant analysis for spectral-spatial classification of hyperspectral images. *IEEE Geoscience and Remote Sensing Letters* **14**(11), 2077–2081 (2017)
38. Wen, J., Fang, X., Cui, J., Fei, L., Yan, K., Chen, Y., Xu, Y.: Robust sparse linear discriminant analysis. *IEEE Transactions on Circuits and Systems for Video Technology* **29**(2), 390–403 (2018)
39. Zhang, L., Edraki, M., Qi, G.J.: Cappronet: Deep feature learning via orthogonal projections onto capsule subspaces. In: *Advances in Neural Information Processing Systems*. pp. 5814–5823 (2018)
40. Zheng, Y., Liu, D., Ren, Q., Sun, B., Niu, Z.: Object tracking via null-space discriminative projections and sparse representation. In: *Proceedings of the International Conference on Video and Image Processing*. pp. 243–248 (2017)